Konya Mühendislik Bilimleri Dergisi, c. 13, s. 1, 294-306, 2025
Konya Journal of Engineering Sciences, v. 13, n. 1, 294-306, 2025
ISSN: 2667-8055 (Electronic)
DOI: 10.36306/konjes.1610031

COPPER EXTRACTION FROM DEEP EUTECTIC SOLVENT AS ATACAMITE BY HYDROLYSIS METHOD

*** Mehmet Ali TOPÇU**

Karamanoğlu Mehmetbey University, Engineering Faculty, Metallurgical and Materials Engineering Department, Karaman, TÜRKİYE
topcumali@kmu.edu.tr

Highlights

- Copper was extracted from deep eutectic solvent with hydrolysis method.
- Atacamite particles with irregular shape was obtained by easy and applicable method.
- Experimental analysis confirmed the crystallinity with and orthorhombic strucutre.
- Optical analysis revealed a band-gap energy of 2.72 eV for atacamite particles.

***Corresponding Author:** Mehmet Ali TOPÇU, topcumali@kmu.edu.tr

Konya Mühendislik Bilimleri Dergisi, c. 13, s. 1, 294-306, 2025
Konya Journal of Engineering Sciences, v. 13, n. 1, 294-306, 2025
ISSN: 2667-8055 (Electronic)
DOI: 10.36306/konjes.1610031

COPPER EXTRACTION FROM DEEP EUTECTIC SOLVENT AS ATACAMITE BY HYDROLYSIS METHOD

*** Mehmet Ali TOPÇU**

Karamanoğlu Mehmetbey University, Engineering Faculty, Metallurgical and Materials Engineering Department, Karaman, TÜRKİYE
topcumali@kmu.edu.tr

(Received: 30.12.2024; Accepted in Revised Form: 13.02.2025)

ABSTRACT: Deep eutectic solvents (DESs) have garnered as promising alternatives to conventional solvents for metal extraction due to their facile synthesis, high chloride concentration, non-aqueous nature, and low cost. This work explores a green route for ultrafast extraction of atacamite [$Cu_2Cl(OH)_3$] from a deep eutectic solvent at room temperature in a short time using copper (II) sulfate pentahydrate as a precursor. The phase, chemical, morphological, and structural properties of the extracted atacamite were investigated using XRD, Rietveld method, SEM-EDX, and FTIR techniques. As a result of XRD analysis, it was determined that the atacamite with an average diameter of 85.59 μm has an orthorhombic crystal structure. Also, it was determined that the crystal structure parameters obtained from XRD and the theoretical calculations of these values were in good agreement according to the Rietveld refinement. SEM/EDX analysis showed that the extracted atacamite particles exhibited heterogeneity in terms of size and morphology, while elemental composition was found to be homogeneous throughout the particles. UV-Vis analysis and theoretical calculations, the optical band of atacamite particles was found as 2.72 eV. Also, this study demonstrates that the hydrolysis method can serve as an efficient, low-energy pathway for the recovery of metals from DESs, highlighting its potential as a novel approach in copper metallurgy.

Keywords: *Deep Eutectic Solvent, Copper Extraction, Atacamite, Rietveld Refinement, Hydrolysis, Characterization*

1. INTRODUCTION

Copper extraction predominantly occurs from sulfide ores, with notable examples including chalcopyrite, bornite, covellite, digenite, and chalcocite. Chalcopyrite represents the most abundant copper mineral, comprising approximately 70% of global copper reserves. Pyrometallurgy has historically been the primary method for copper extraction, but this method is economically viable only for high-grade ores and poses significant environmental challenges due to substantial SO_2 emissions. Therefore, hydrometallurgy has emerged as an alternative method for extracting copper from sulfidic copper ores, which is particularly advantageous for processing low-grade copper ores due to its lower operational expenditures [1], [2].

Hydrometallurgy is an aqueous-based metallurgical process utilized for the recovery of metals from ores or industrial residues. The process involves the leaching of metal-bearing materials using suitable aqueous reagents, including acidic, basic, or saline solutions, to extract metal ions into the solution. Subsequently, the metal ions in the solution are recovered in their metallic or compound form through various techniques such as precipitation, ion exchange, cementation, and electrodeposition. Because it consumes less energy and is more environmentally friendly than pyrometallurgical methods, hydrometallurgical methods have gained popularity, they are not without drawbacks. These processes often involve lengthy procedures, lower metal recovery rates, and significant consumption of strong acids. Additionally, wastewater discharge can lead to secondary pollution. The shortcomings of the conventional methods have spurred the development of solvometallurgy as a novel and attractive approach [3], [4].

***Corresponding Author:** Mehmet Ali TOPÇU, topcumali@kmu.edu.tr

Despite the solvent-related differences between solvometallurgy and hydrometallurgy, many of the unit operations show similarities. Solvometallurgy is a process that uses non-aqueous solvents such as ionic liquids, deep eutectic solvents (DESs), liquefied ammonia, concentrated sulfuric acid or, supercritical carbon dioxide to dissolve minerals or wastes at lower temperatures, enabling metal recovery [5], [6]. Over the past few years, in search of green solvents that can replace harmful and volatile organic solvents, researchers have shown great interest in deep eutectic solvents (DESs) which stand out with their low melting point, low vapor pressure, high solubility, non-flammability, negligible toxicity, and easily recyclable properties [7]. DESs are defined as a stable eutectic system formed by mixing two or more components, resulting in a significantly lower eutectic point temperature compared to an ideal liquid mixture. They are generally produced by the formation of strong hydrogen bonds between hydrogen bond donor molecules (HBDs) and hydrogen bond acceptor molecules (HBAs). Charge delocalization from the interaction of HBDs with quaternary ammonium salts triggers the formation of DES, causing a significant decrease in the melting point. The melting point of the eutectic mixture is lower than the melting point of its constituent pure HBDs and HBAs components or an ideal liquid mixture. Various DESs can be synthesized including binary, ternary, and quaternary DESs can be synthesized by combining a large number of HBAs and HBDs components. The first DES synthesized by Abbott et al., was obtained by mixing the components choline chloride as HBA with a melting point of 302 ºC and urea as HBD with a melting point of 133 ºC in specific proportions. The melting point of this mixture is 12 ºC and it forms a stable, transparent liquid at room temperature [8]. DESs are typically represented by the general formula $Cat^{+}X^{-}zY$, where Cat^{+} denotes an organic anion (e.g., ammonium, sulfonium, or phosphonium); X^{-} is a halide anion acting as Lewis's base, Y is Brønsted or Lewis acid, and z signifies the number of Y molecules interacting with the X^{-} anion. For example, choline chloride (ChCl, $[HOC_2H_4N(CH_3)_3^{+}Cl]$), the most commonly used HBA, forms complexes with HBDs of the following reaction [9], [10].

$$[Ch^{+}][Cl^{-}]+HBD \rightarrow [Ch^{+}]+HBDCl^{-} \quad (1)$$

Due to their unique physicochemical properties, deep eutectic solvents (DESs) have emerged as promising alternatives to conventional solvents for metal recovery and other applications [11], [12]. Thanks to the customizable structures of DESs, special solvers can be designed for different applications. DESs have potential applications in many fields such as metal extraction, extraction of biological molecules, catalysis, electrochemistry, and materials science. In particular, important studies are being carried out in areas such as selective separation and recovery of metal ions, extraction of active ingredients in the pharmaceutical industry, and synthesis of nanomaterials [13], [14].

The increasing demand for metals is driven by technological advancements, and the development of more efficient and greener methods for metal recovery from low-grade ores, industrial waste, and by-products. Thus far, numerous studies have been conducted on the recovery of various metals such as lead, zinc, cobalt, lithium etc., from different sources including ore or metallurgical waste, using solvometallurgical leaching [15], [16]. The applications of DESs to copper recovery have yielded promising results in copper metallurgy. Angarra et al., investigated the electrochemical dissolution and recovery of chalcopyrite mineral in different DESs. A mixed DES, comprising 20 wt% ChCl-oxalic acid and 80 wt% ChCl-ethylene glycols, yielded the highest selective copper recovery (99%) from chalcopyrite, as reported by researchers [17]. Zhao et. al., investigated the extraction of copper from an end-of-life circuit board using three ChCl-based DESs synthesized with ethylene glycol, oxalic acid, and glycol acid. The results indicated that 90.35% Zn, 87.47% Pb, and 16.77% Cu were extracted from the blended metal powder through calcination and leaching with ChCl-glycol acid [18]. Topçu et. al., studied copper recovery from copper smelting slag with ChCl-urea DES as a green reagent. Experimental findings showed that 80% of copper leaching can be achieved at 48 h, 95 °C, 1/25 $g \cdot ml^{-1}$, and -33 μm [19]. Although studies on copper recovery from various sources have yielded promising results, research on copper extraction from DESs solutions remains limited.

In addition to the extraction of copper from natural sources, synthetic production of copper minerals has been investigated previously. Atacamite, widely utilized in catalysis, pigment and dye production, and the pharmaceutical industry due to its antifungal properties, has been synthesized using various techniques [20]. Xie et al., have synthesized atacamite as precursor for the production of CuO. The synthesis of the atacamite precursor commenced by the dropwise addition of 50 mL of a 0.7 M mixed solution of KOH and K_2CO_3 to 20 mL of a vigorously stirred, hot 3.5 M $CuCl_2$ solution. The reaction was accompanied by the evolution of gas bubbles and the formation of a bluish-green precipitate. The precipitate was subsequently isolated through successive centrifugation and washing steps, employing distilled water and ethanol as washing solvents. The collected precipitate was then dried overnight at 60 °C in a desiccator. In the subsequent step, 20 mL of a 2 M KOH aqueous solution was added dropwise to a 5 mL suspension containing 0.3 g of the previously synthesized atacamite precursor under continuous stirring. This addition resulted in the formation of a blue precipitate [21]. Zhu et al., prepared atacamite nanoribbons following three step reaction process. Aqueous solutions of $CuCl_2{\cdot}2H_2O$ and $(NH_4)_2CO_3$ were prepared at specific concentrations. Subsequently, the $CuCl_2$ solution was added dropwise to a vigorously stirred solution of $(NH_4)_2CO_3$. Upon mixing, an initial white precipitate formed, which subsequently dissolved. As the molar ratio of $CuCl_2{\cdot}2H_2O$ to $(NH_4)_2CO_3$ approached 1:2, a characteristic deep blue complex solution was observed. This solution was then aged for 2-7 days, resulting in the formation of a jade-green precipitate of $Cu_2Cl(OH)_3$. The precipitate was isolated by centrifugation, washed thoroughly with distilled water and ethanol, and finally dried in an oven at 60 °C for 12 hours [22]. Nascimento et al., investigated the structural and antifungal properties of β-atacamite samples synthesized via a sonochemical driven route. The synthesis of atacamite was initiated by dissolving 1 mmol of copper chloride dihydrate and 2 mmol of sodium chloride in 40 mL of distilled water. Simultaneously, 0.5 mmol of calcium carbonate ($CaCO_3$) was dissolved in a separate container. Subsequently, the solution containing copper and chloride ions was poured into a beaker containing 50 mL of a freshly prepared urea hydrolysis solution. The mixture was sonicated at 2000 W, 20 kHz, with an amplitude of 60%, using a pulse cycle of 5 seconds on and 10 seconds off. The mixture was then added dropwise to the solution containing calcium ions, resulting in the immediate formation of a light green suspension under sonication at room temperature [23].

This study investigated copper extraction from a DES formulated with ChCl and urea, two readily available, cost-effective, and biocompatible components, exhibiting high copper solubility and metal-free composition. After dissolving the copper bearing mineral, hydrolysis method was performed to obtain copper as atacamite particles at room temperature. Also, the chemical, mineralogical, and optical properties of extracted particles were revealed by detailed quantitative analyses.

2. MATERIAL AND METHODS

Copper (I) sulfate pentahydrate ($CuSO_4.5H_2O$, >98%) was used in this work provided from Sigma Aldrich. Deep eutectic solvent was prepared using commercially available choline chloride ChCl, $C_5H_{14}ClNO$) and urea ($CO(NH_2)_2$, >99% purity) supplied by Merck without any prior purification steps. The deionized water used in the hydrolysis experiment was obtained from the MP MINIPure brand water device.

40 mmol ChCl (5584.8 mg ChCl) and 80 mmol urea (4804.8 mg) (stoichiometric molar ratio of 1:2) were mixed in a 50 ml glass bottle. Then, the mixture was subjected to gentle heating to 50 ºC using a temperature-controlled hot plate and stirred (250 rpm) continuously until a homogeneous colourless liquid was obtained. The solution was subsequently cooled and placed in a desiccator for further metal extraction experiments. The formation of deep eutectic solvent is illustrated in **Fig.1.a**.

The dissolving process of $CuSO_4.5H_2O$ was carried out in DES solution at 50 ºC. 2 g of $CuSO_4.5H_2O$ was added to 25 mL of DES solution and the mixture was stirred until the sample was completely dissolved. Then, the distilled water was added dropwise until the solution became turbidite and white particles were produced. After the hydrolysis experiment, solid and liquid parts were separated using a centrifuge. Following separation, the green solid particles were washed with acetone to eliminate

organic contaminants and dried at 50 ºC before characterization.

The phase analysis of the precipitated sample was detected with X-ray diffraction analysis (XRD, Bruker Advance D8). Phase identification and quantification were conducted using Panalytical HighScore Plus@, which utilizes the International Centre for Diffraction Data (ICDD) database. A scanning electron microscope (SEM, Hitachi SU5000) with an energy dispersive X-ray module (EDX) was used to monitor the morphological properties and chemical composition of the samples. The structural properties of copper precipitates were detected with fourier transform infrared spectroscopy (FT-IR). FT-IR analysis was carried out using Bruker Vertex 70 ATR-FTIR over the range 4000 – 400 cm^{-1} with a nominal resolution of 8 cm^{-1}. The optical properties of atacamite particles were examined by UV-Vis absorption spectroscopy recorded on a Shimadzu UV 2600 UV-Vis spectrometer. The experimental works are illustrated in **Fig. 1.b.**

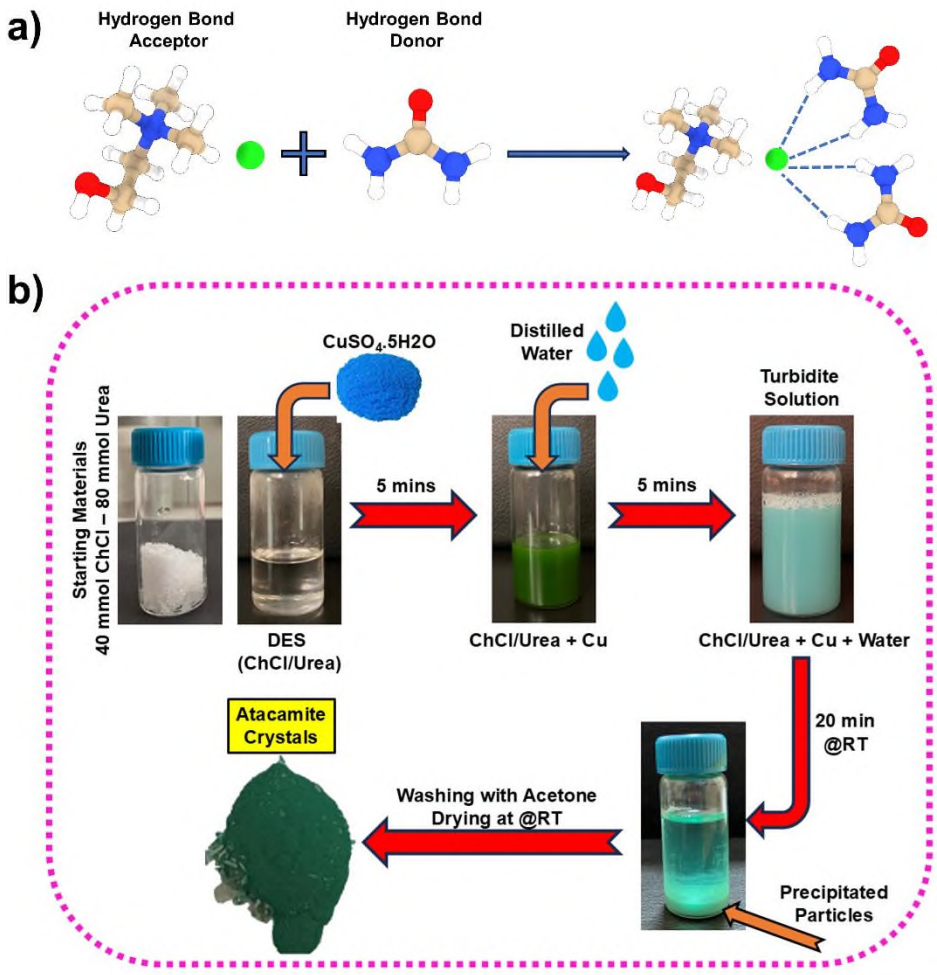

Figure 1. a) Formation of deep eutectic solvent and **b)** flow chart of experimental processes

3. RESULTS AND DISCUSSION

Phase properties of extracted particles from DES solution were investigated by X-ray diffraction technique. As seen from the XRD pattern (**Fig 2a**.), the particles extracted from DES solution at room temperature were $Cu_2Cl(OH)_3$ according to the JCPDS card number 96-900-7719. The position of main diffraction peaks at 16.15º, 16.63º, 32.19º, 39.67º, 50.04º, 52.62º, and 67.86º are indexed with (011), (101), (013), (004), (033), (105), and (026) planes of the orthorhombic crystal structure with space group Pnma 62.

The mechanisms underlying metal dissolution using DESs have been the subjects of recent

investigations. A two-step mechanism is commonly proposed for the dissolution of metal oxides in DES. (*i*) the dissolution mechanism of metal oxides in DES is considered to initiate with an interaction between the protons of the functional groups within HBD (e.g., carboxyl groups in organic acids, hydroxyl groups in alcohols) and the active hydroxyl sites on the hydrated metal species surface, leading to the formation of intermediate species with protonated oxide, which can be expressed by the following equation [15], [24] :

$$Bulk \equiv Me - OH + HX \leftrightarrow bulk \equiv Me - OH_2^+ \cdots X^{n-} \quad (2)$$

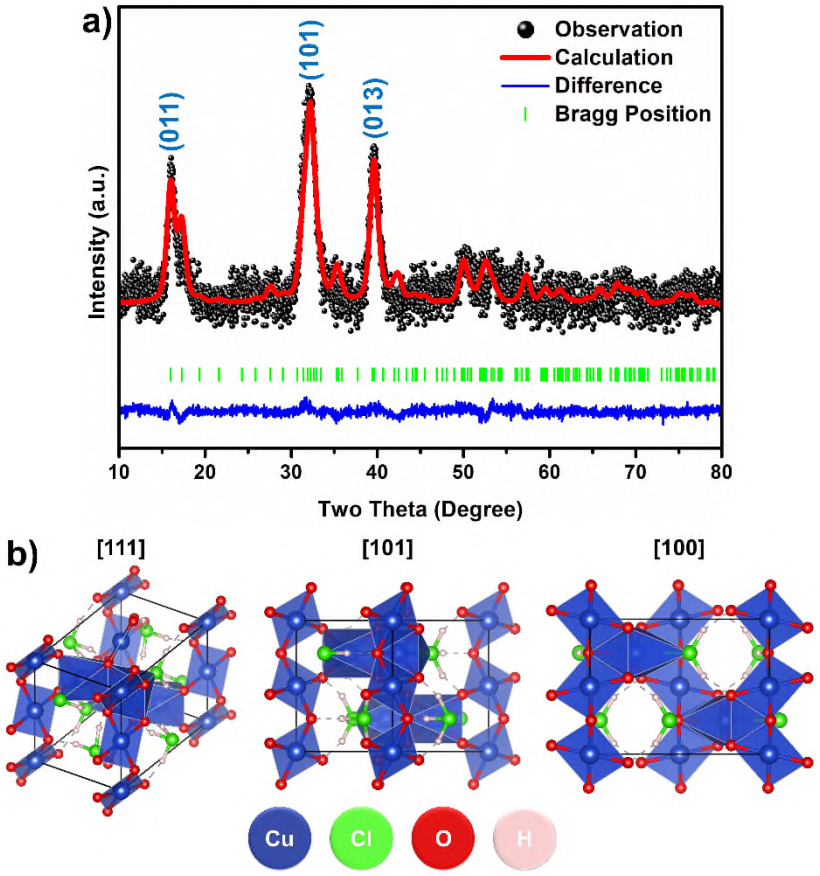

Figure 2. a) Rietveld refinement XRD graph and **b)** illustration of the crystal structure of atacamite

where Bulk ≡ Me-OH denotes a hydrated metal oxide with active OH sites; HX is the HBDs of DES.

(ii) If the metal-ligand complexes are thermodynamically more stable than the metal-hydroxide complexes, the protons would preferentially interact with the oxide anions, leading to the cleavage of metal oxide bonds. Deprotonated HBD ligands can substitute the active hydroxyl sites of the metal oxide, promoting metal-ligand complexation. Subsequently, anionic species (Cl^-) within the bulk DES may engage in ligand exchange anions reactions.

$$Bulk \equiv Me - OH_2^+ \cdots X^{n-} \leftrightarrow Me - X_{(DES)}^{n-} + H_2O \quad (3)$$

The dissolution process of metal species involves the availability of protons from HBD in the DES prepared with ChCl and urea. The protons facilitate the dissolution of metal species by weakening the metal-oxygen bonds through the protonation of the oxide anions. Furthermore, the chloride anions supplied by the HBA can significantly contribute to the stabilization of the dissolved metal ions through

the formation of metal-chloro complexes. It has been previously reported that the dissolution of both oxide and sulfide metal species in ChCl-urea DES invariably results in the formation of metal complexes in the final solution. Consequently, it can be inferred that the dissolving of $CuSO_4.5H_2O$ using the ChCl-urea mixture results in the formation of $[CuClO.urea]^-$ complex anions within the solution.

$$CuSO_4.H_2O + ChCl/urea \rightarrow [CuClO.urea]^- + Ch^+ + SO_4 + H_2O \quad (4)$$

Upon the addition of water to the DES solution, the decomposition of urea in the CuClO/urea complex will hydroxide anions (Eq 5). Subsequently, atacamite particles will form in the presence of high concentration of chloride and hydroxide anions (Eq. 6) [25] .

$$CO(NH_2)_2 + 3H_2O \rightarrow 2NH_4^+ + CO_2 + 2OH^- \quad (5)$$

$$2Cu^{2+} + 3OH^+ + Cl^- \rightarrow Cu_2Cl(OH)_3 \quad (6)$$

Rietveld refinement analysis was employed to comprehensively determine the crystallographic parameters of the precipitated using Panalytical HighScore Plus software. **Fig. 2.b** also illustrates the outcome of Rietveld refinement, displaying the experimentally observed XRD pattern (Y_{obs}), the calculated diffraction pattern (Y_{calc}), the difference plot between the observed and calculated intensities (Y_{obs} - Y_{calc}), and the position of Bragg reflections. Theoretical calculations were performed to investigate the crystal structure, which was assigned to the Pnma 62 space group. The Rietveld refinement procedure yielded a set of goodness-of-fit parameters, including the weighted profile factor (R_{wp}), the expected weighted profile factor (R_{exp}), the Bragg R-factor (R_{Bragg}), the crystallographic R-factor (R_{cryst}), the chi-square value (χ^2), and the overall goodness-of-fit index (GoF). These values are presented in **Table 1**.

The χ^2 [$(R_{wp}/R_{exp})^2$] and GoF (R_{wp}/R_{exp}) values were obtained as 0.01326 and 0.1151, respectively, and these parameters show the quality of refinement. The goodness fit parameters χ^2 and GoF are below 1, indicating the reliability of the refinement method [26], [27]. Also, a comparative analysis of the lattice parameters, as determined by Rietveld refinement, is provided in **Table 1**. A comparison between the lattice parameters derived from Rietveld refinement and XRD patterns with theoretical values reveals an excellent agreement. The crystallographic illustration of the orthorhombic structure belonging to atacamite is presented in **Fig.3(b)**. The unit cell of the orthorhombic crystal system consists of 95 atoms, 120 bonds, and 19 polyhedra. There are two inequivalent Cu^{+2} sites in orthorhombic crystallizes structure. In the first Cu^{2+} site, the copper cation (Cu^{2+}) is coordinated in a distorted square plane geometry by four oxygen anions and two equivalent chloride anions. The Cu-O bonds display a distinct asymmetry, featuring two shorter bonds of 1.95 Å and two longer bonds of 1.99 Å. In contrast, the two Cu-Cl bonds are of equal length at 2.91 Å. The second Cu^{2+} ion occupies a six-coordinate site, being bonded to five oxygen anions and one chloride ion. The Cu-O bonds display a heterogeneity in bond lengths, varying from 2.01 Å to 2.38 Å. The Cu-Cl bond, however, exhibits a more uniform length of 2.88 Å. Besides the copper ion sites, there are two inequivalent H^{+1} sites. The primary hydrogen center exhibits a linear coordination geometry, wherein it is coordinated to one oxide ion and one chloride ion. The H-O bond length is determined to be 0.99 Å, and the H-Cl bond length is experimentally determined to be 2.06 Å. The secondary hydrogen cation (H^+) occupies a linear coordination site, bonded to one oxygen anion (O^{-2}) and one chloride anion (Cl^-). The H-O bond length is 1.00 Å, while the H-Cl bond length is 2.05 Å. Two distinct oxygen anion sites are observed. The primary O^{-2} site exhibits a distorted coordination geometry, bonded to three Cu^{+2} cations and one H^+ cation. Similarly, the secondary O^{-2} site is also distorted, coordinating to three Cu^{+2} cations and one H^+ cation. The chloride anion (Cl^-) adopts a six-coordinate geometry, forming bonds with three Cu^{+2} cations and three H^+ cations.

Table 1. Rietveld refinement parameters and lattice constant of atacamite

R_{wp}	R_{exp}	R_{Bragg}	R_{Cryst}	χ^2	Gof
9.76	84.76	4.21	3.7	0.01326	0.1151
Lattice Constant	**Theoritical**	**Rietveld**	**XRD**		
a (Å)	6.02797	6.08314	6.05288		
b (Å)	6.86383	6.80939	6.78210		
c (Å)	9.11562	9.01706	9.01193		
Volume $(Å)^3$	377.158	373.509	369.950		

The extraction efficiency of the proposed method was determined by comparing the initial mass of the starting material, $CuSO_4.5H_2O$ (2 g), with the final mass of the extracted atacamite (1.334 g). The copper content of the $CuSO_4.5H_2O$:

$$= \frac{[2\ g\ CuSO_4.5H_2O]\ x\left[65.546\ {}^{g}/_{mol}\ Cu\right]}{\left[294.685\ {}^{g}/_{mol}\ CuSO_4.5H_2O\right]} = 0.445\ g\ Cu \quad (7)$$

The copper content of the extracted atacamite:

$$= \frac{[0.670\ g\ Cu_2Cl(OH)_3]\ x\left[2\ x\ 65.546\ {}^{g}/_{mol}\ Cu\right]}{\left[213.57\ {}^{g}/_{mol}\ Cu_2Cl(OH)_3\right]} = 0.410\ g\ Cu \quad (8)$$

The extraction efficiency of the proposes method:

$$= \left(\frac{0.410\ g\ Cu}{0.445\ g\ Cu}\right) x\ 100 = 92.1\% \quad (9)$$

The morphological properties of the extracted atacamite were analyzed by SEM/EDX as shown in **Fig. 3(a-d)**.

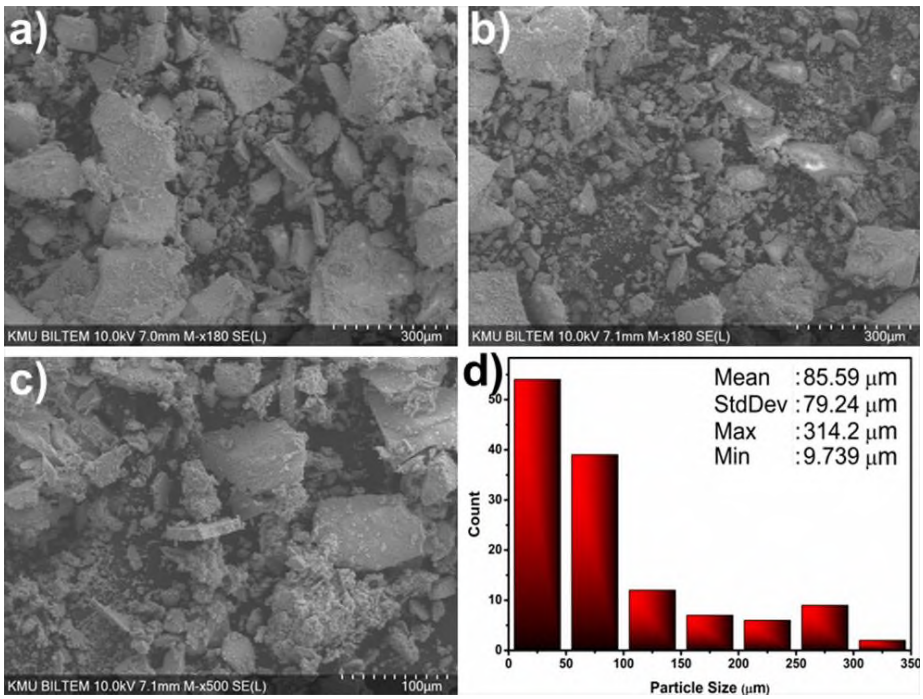

Figure 3. (a-c) SEM images and **d)** particle size disrubition of atacamite particles

The atacamite particles extracted from the DES medium exhibited a variety of sizes and morphologies, as observed in SEM images. SEM analysis indicated the presence of particles with diverse

morphologies, encompassing plate-like, spherical, and rod-like structures. According to the particle size analysis, the average size of the atacamite particles was determined to be 85.59 μm. Despite the presence of particles as large as 314.2 μm, particle size analysis revealed that a majority of the atacamite particles obtained from the DES solution were smaller than 50 μm (**Fig. 3.d**).

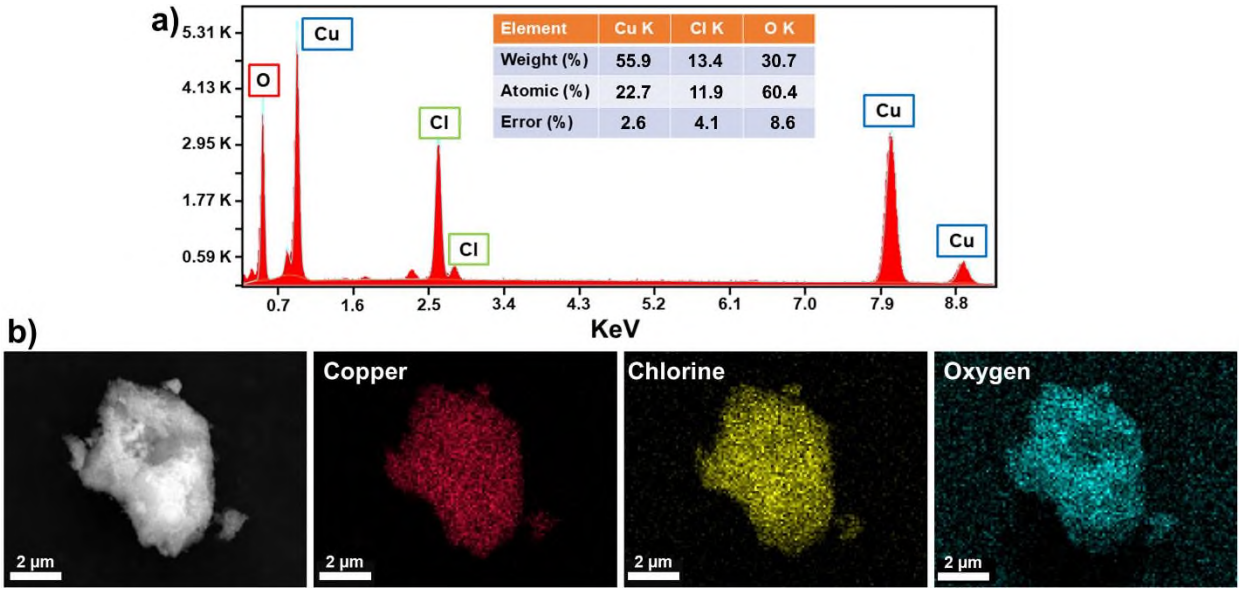

Figure 4. b) EDX analysis and **b)** elemental mapping of atacamite powders

The chemical composition and elemental mapping results obtained with EDX analysis are shown in **Fig. 4(a-b)**. The EDX spectrum exhibits intense peaks corresponding to copper, chlorine, and oxygen (**Fig. 4.a**). The elemental composition of atacamite, as determined by EDX analysis, is inconsistent with theoretical values. Stoichiometrically, the atacamite mineral is composed of 59.51% copper, 22.47% oxygen, 16.60% chlorine, and 1.42% hydrogen. In the elemental mapping, copper, chlorine, and oxygen are represented by red, yellow, and blue, respectively. It is apparent from **Fig. 4.b** that copper, chlorine, and oxygen have been homogeneously distributed throughout the particles.

FTIR spectroscopy was utilized to investigate the chemical composition and bonding characteristics of atacamite particles. **Fig. 5**. shows the typical FTIR spectra of the extracted atacamite particles. The atacamite particles exhibited high-intensity infrared bands in the region of 3346 – 3324 cm^{-1}, attributable to hydroxyl stretching vibration groups with different Cu-O distances. The bands observed at 1644 and 1631 cm^{-1} are attributed to O-H bending vibrations. Additionally, The FTIR spectrum also revealed six distinct infrared bands at 983, 948, 918, 894, and 846 cm^{-1}, corresponding to vibrational modes influenced by interactions between Cu-O-H and O-H···Cl groups. The intense bands observed below 820 cm^{-1} are assigned to the Cu-O stretching vibrational modes within the crystal structure [23], [25].

UV-Vis analysis was employed to investigate the optical properties of extracted atacamite particles with the results presented in **Fig. 6(a-d)**. **Fig. 6.a** demonstrates a gradual increase in reflectivity for atacamite derived from DES solution as the wavelength increases from the ultraviolet to the visible range. The maximum reflectivity was observed in the near-infrared region. The band gap and its nature in atacamite particles were determined using diffuse reflectance spectroscopy data. Initially, the absorption, expressed as the Kubelka-Munk function F(R∞) was calculated using Eq. 10.

$$F(R_\infty) = \frac{(1-R)^2}{2R} \tag{10}$$

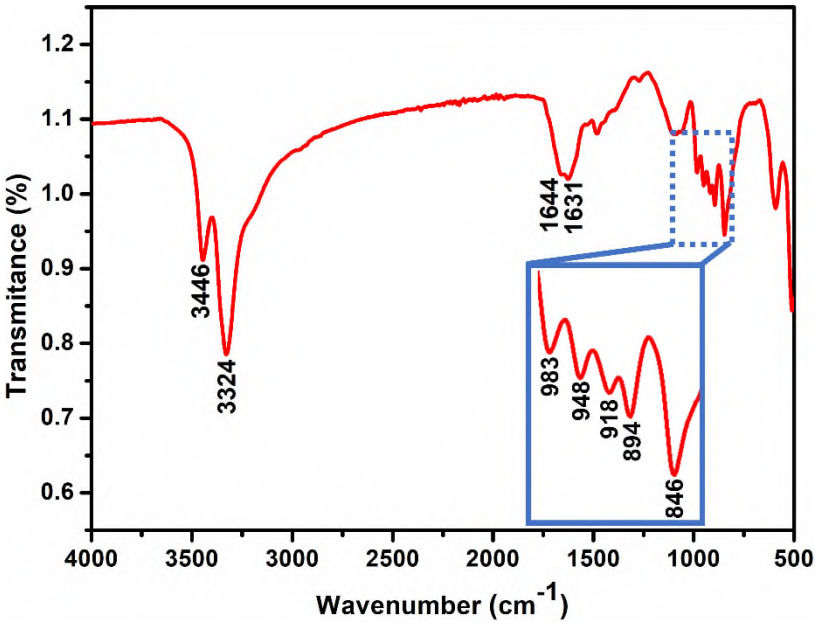

Figure 5. FTIR spectra of atacamite particles

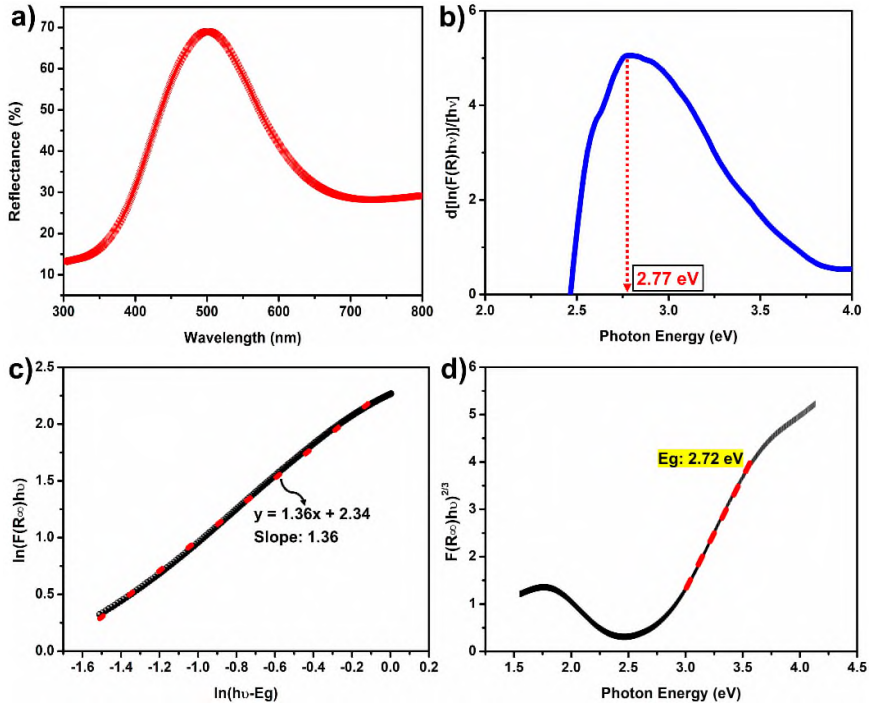

Figure 6. (a) Diffuse reflectance, **(b)** d[ln(F(R∞)hυ)]/[hυ] vs. photon energy graph, **(c)** ln(F(R∞)hυ) vs. ln(hυ-E_g) graph, and **(d)** band-gap energy diagram of atacamite particles

where F(R∞) is the Kubelka-Munk function relates to absorption and R represents the percent.

According to the *d[ln(F(R∞)hυ)]/[hυ]* vs. photon energy graph (**Fig. 6.b**), the band gap was estimated to be approximately 2.77 eV based on absorption data. The Tauc's equation (Eq. 11) was employed to determine the *m* exponent, obtained from the slope of the *ln (F(R∞)hυ)-ln(hυ-Eg)* plot (**Fig. 6.c**), which provides information about the type of electron transitions. The *m* value was found to be 1.36 and this

reveals that atacamite particles have forbidden direct transition type.

$$F(R_\infty)h\upsilon = A(h\upsilon - EG)^m \quad (11)$$

where $h\upsilon$ represents the photon energy, A is the material-specific constant, Eg is the optical band gap and m is the exponent that characterizes the type of band gap.

Thus, the optical band-gap of atacamite particles was estimated as 2.72 eV by fitting the linear part of the $(F(R\infty)h\upsilon)^{2/3}$ vs. the photon energy graph (**Fig. 6.d**). When the optical properties of atacamite extracted from DES solution were compared to those reported in the literature, a good agreement was found [23], [28].

The experimental results presented herein strongly support the feasibility of employing the proposed methods in copper metallurgy. Given its simplicity, cost-effectiveness, and minimal environmental impact, the hydrolysis method offers a sustainable and energy-efficient approach for recovering copper from DES leach solution resulting in the formation of atacamite. Copper-containing materials exhibit a wide range of properties making them suitable for applications such as photocatalysis, antibacterial coating, and the development of biosensors and electrochemical sensors. The rich chemistry of copper has facilitated its incorporation into a diverse range of natural minerals and biological systems. The tribasic copper chloride mineral family [$Cu_2(OH)Cl$] has attracted considerable interest owing to its structural diversity and potential applications in various technological domains. Stoichiometric $Cu_2(OH)_3Cl$ exists in multiple polymorphs including atacamite (orthorhombic), botallackite (monoclinic), and clinoatacamite (monoclinic). The unique combination of geometric frustration and unconventional magnetic properties in $Cu_2(OH)_3Cl$ has driven significant interest in this material for fundamental studies [28], [29]. $Cu_2(OH)_3Cl$ materials with diverse crystal structures are commonly synthesized via hydrothermal methods involving the use of aqueous solvents and mineralizers under high temperatures and pressure, requiring additional equipment and energy [28], [30]. The proposed hydrolysis method in this study offers a simple, low-cost, and environmentally friendly approach to synthesizing atacamite particles at room temperature, eliminating the need for additional equipment.

4. CONCLUSIONS

Atacamite was successfully recovered from DES solution using a simple, low-cost, and fast route at ambient temperature. XRD analysis confirmed the formation of highly crystalline $Cu_2(OH)Cl$ with an orthorhombic structure (Pnma), demonstrating rapid and efficient synthesis within a short extraction time. SEM images show the presence of particles with an average size of 89.5 μm with irregular morphologies. EDX spectra indicate that the extracted particles contain predominantly copper, chlorine, and oxygen elements. FTIR analysis showed the presence of typical characteristic bands of atacamite. Diffuse reflectance spectroscopy measurements and mathematical calculations determined the optical bandgap of atacamite microparticles to be 2.77 eV. The facile nature of the hydrolysis method positions it as a viable strategy for the solvometallurgical recovery of valuable metals from complex matrices such as DES. Furthermore, this work offers a practical approach to the synthesis of atacamite at room temperature with simple, fast, and environmental compatibility.

Declaration of Ethical Standards

The author followed all ethical guidelines, including authorship, citation, data reporting, and publishing original research.

Declaration of Competing Interest

The author declares that they have no known competing financial interest or personal relationships

that could have appeared to influence the work reported in this paper.

Funding / Acknowledgements

The authors declares that there is no financial support.

Data Availability

No data was used for the research described in the article.

REFERENCES

[1] J. Hu, F. Zi, and G. Tian, "Extraction of copper from chalcopyrite with potassium dichromate in 1-ethyl-3-methylimidazolium hydrogen sulfate ionic liquid aqueous solution," *Minerals Engineering*, vol. 172, p. 107179, 2021, doi: https://doi.org/10.1016/j.mineng.2021.107179

[2] G. Ji, Y. Liao, Y. Wu, J. Xi, and Q. Liu, "A review on the research of hydrometallurgical leaching of low-grade complex chalcopyrite," *Journal of Sustainable Metallurgy*, vol. 8, no. 3, pp. 964–977, 2022, doi: https://doi.org/10.1007/s40831-022-00561-5

[3] L. Xiao et al., "An environmentally friendly process to selectively recover silver from copper anode slime," *Journal of Cleaner Production*, vol. 187, pp. 708–716, 2018, doi: https://doi.org/10.1016/j.jclepro.2018.03.203

[4] K. Binnemans and P. T. Jones, "The twelve principles of circular hydrometallurgy," *Journal of Sustainable Metallurgy*, vol. 9, no. 1, pp. 1–25, 2023, doi: https://doi.org/10.1007/s40831-022-00636-3

[5] X. Li, W. Monnens, Z. Li, J. Fransaer, and K. Binnemans, "Solvometallurgical process for extraction of copper from chalcopyrite and other sulfidic ore minerals," *Green Chemistry*, vol. 22, no. 2, pp. 417–426, 2020, doi: https://doi.org/10.1039/C9GC02983D

[6] K. Kurniawan, S. Kim, M. Bae, A. Chagnes, and J. Lee, "Investigation on solvometallurgical processes for extraction of metals from sulfides," *Minerals Engineering*, vol. 218, p. 109005, 2024, doi: https://doi.org/10.1016/j.mineng.2024.109005

[7] K. A. Omar and R. Sadeghi, "Physicochemical properties of deep eutectic solvents: A review," *Journal of Molecular Liqiud*, vol. 360, p. 119524, 2022, doi: https://doi.org/10.1016/j.molliq.2022.119524

[8] A. P. Abbott, G. Capper, D. L. Davies, R. K. Rasheed, and V. Tambyrajah, "Novel solvent properties of choline chloride/urea mixtures," *Chemical Communications*, no. 1, pp. 70–71, 2003, doi: https://doi.org/10.1039/B210714G

[9] A. P. Abbott, G. Capper, D. L. Davies, K. J. McKenzie, and S. U. Obi, "Solubility of metal oxides in deep eutectic solvents based on choline chloride," *Journal of Chemical & Engineering Data*, vol. 51, no. 4, pp. 1280–1282, Jul. 2006, doi: https://doi.org/10.1021/je060038c

[10] A. P. Abbott, D. Boothby, G. Capper, D. L. Davies, and R. K. Rasheed, "Deep eutectic solvents formed between choline chloride and carboxylic acids: Versatile alternatives to ionic liquids," *Journal of the American Chemical Society*, vol. 126, no. 29, pp. 9142–9147, Jul. 2004, doi: https://doi.org/10.1021/ja048266j

[11] N. Peeters, K. Binnemans, and S. Riaño, "Solvometallurgical recovery of cobalt from lithium-ion battery cathode materials using deep-eutectic solvents," *Green Chemistry*, vol. 22, no. 13, pp. 4210–4221, 2020, doi: https://doi.org/10.1039/D0GC00940G

[12] Q. Zhang, K. De Oliveira Vigier, S. Royer, and F. Jérôme, "Deep eutectic solvents: syntheses, properties and applications," *Chemical Society Reviews*, vol. 41, no. 21, pp. 7108–7146, 2012, doi: https://doi.org/10.1039/C2CS35178A

[13] B. B. Hansen et al., "Deep eutectic Solvents: A review of fundamentals and applications," *Chemicals Reviews*, vol. 121, no. 3, pp. 1232–1285, Feb. 2021, doi: https://doi.org/10.1021/acs.chemrev.0c00385

[14] T. El Achkar, H. Greige-Gerges, and S. Fourmentin, "Basics and properties of deep eutectic solvents: a review," *Environmental Chemistry Letters*, vol. 19, no. 4, pp. 3397–3408, 2021, doi: https://doi.org/10.1007/s10311-021-01225-8

[15] S. Suffia and D. Dutta, "Applications of deep eutectic solvents in metal recovery from E-wastes in a sustainable way," *Journal of Molecular Liqiud*, vol. 394, p. 123738, 2024, doi: https://doi.org/10.1016/j.molliq.2023.123738

[16] M. I. Martín, I. García-Díaz, and F. A. López, "Properties and perspective of using deep eutectic solvents for hydrometallurgy metal recovery," *Minerals Engineering*, vol. 203, p. 108306, 2023, doi: https://doi.org/10.1016/j.mineng.2023.108306

[17] S. Anggara et al., "Direct extraction of copper from copper sulfide minerals using deep eutectic solvents," *Green Chemistry*, vol. 21, no. 23, pp. 6502–6512, 2019, doi: https://doi.org/10.1039/C9GC03213D

[18] Q. Zhao, S. Ma, W. Ho, Y. Wang, J. Y. T. Ho, and K. Shih, "Simple and environmentally friendly metal recovery from waste printed circuit boards by using deep eutectic solvents," *Journal of Cleaner Production*, vol. 421, p. 138508, 2023, doi: https://doi.org/10.1016/j.jclepro.2023.138508

[19] M. A. Topçu, S. A. Çeltek, and A. Rüşen, "Green leaching and predictive model for copper recovery from waste smelting slag with choline chloride-based deep eutectic solvent," *Chinese Journal of Chemical Engineering*, vol. 75, pp. 14–24, 2024, doi: https://doi.org/10.1016/j.cjche.2024.07.005

[20] D. Haro, P. García-Muñoz, M. Mola, F. Fresno, and J. Rodríguez-Chueca, "Atacamite ($Cu_2Cl(OH)_3$) as catalyst of different AOPs for water disinfection," *Catalysis Today*, vol. 429, p. 114496, 2024, doi: https://doi.org/10.1016/j.cattod.2023.114496

[21] H. Xie, L. Zhu, W. Zheng, J. Zhang, F. Gao, and Y. Wang, "Microwave-assisted template-free synthesis of butterfly-like CuO through $Cu_2Cl(OH)_3$ precursor and the electrochemical sensing property," *Solid State Sciences*, vol. 61, pp. 146–154, 2016, doi: https://doi.org/10.1016/j.solidstatesciences.2016.09.017

[22] C. Zhu, C. Chen, L. Hao, Y. Hu, and Z. Chen, "Template-free synthesis of $Cu_2Cl(OH)_3$ nanoribbons and use as sacrificial template for CuO nanoribbon," *Journal of Crystal Growth*, vol. 263, no. 1, pp. 473–479, 2004, doi: https://doi.org/10.1016/j.jcrysgro.2003.11.003

[23] M. V. B. do Nascimento et al., "Sonochemical-driven synthesis of synthetic Atacamite - β-$Cu_2(OH)_3Cl$: Structure, and its antifungal activity," *Nano-Structure and Nano-Objects*, vol. 34, p. 100958, 2023, doi: https://doi.org/10.1016/j.nanoso.2023.100958

[24] Z. Yuan, H. Liu, W. F. Yong, Q. She, and J. Esteban, "Status and advances of deep eutectic solvents for metal separation and recovery," *Green Chemistry*, vol. 24, no. 5, pp. 1895–1929, 2022, doi: https://doi.org/10.1039/D1GC03851F

[25] Z. Jie et al., "Fabrication of octahedral Atacamite microcrystals via a hydrothermal route," *Micro and Nano Letters*, vol. 6, no. 3, pp. 119–121, Mar. 2011, doi: https://doi.org/10.1049/mnl.2010.0217

[26] Z. Liu, Y. Zong, H. Li, D. Jia, and Z. Zhao, "Selectively recovering scandium from high alkali Bayer red mud without impurities of iron, titanium and gallium," *Journal of Rare Earths*, vol. 35, no. 9, pp. 896–905, 2017, doi: https://doi.org/10.1016/S1002-0721(17)60992-X

[27] C.-Z. Liao, L. Zeng, and K. Shih, "Quantitative X-ray Diffraction (QXRD) analysis for revealing thermal transformations of red mud," *Chemosphere*, vol. 131, pp. 171–177, 2015, doi: https://doi.org/10.1016/j.chemosphere.2015.03.034

[28] X. Liu, L. Xu, Y. Huang, H. Cheng, and H. J. Seo, "Paratacamite phase stability and improved optical properties of $Cu_2(OH)_3Cl$ crystal via Ni-doping," *Materials & Design*, vol. 121, pp. 194–201, 2017, doi: https://doi.org/10.1016/j.matdes.2017.02.071

[29] M. R. Bisengalieva, I. A. Kiseleva, L. V. Melchakova, L. P. Ogorodova, and A. M. Gurevich, "The molar heat capacity of hydrous copper chloride: atacamite $Cu_2Cl(OH)_3$," *The Journal of Chemical Thermodynamics*, vol. 29, no. 3, pp. 345–352, 1997, doi: https://doi.org/10.1006/jcht.1996.0162

[30] S. Chu, P. Müller, D. G. Nocera, and Y. S. Lee, "Hydrothermal growth of single crystals of the quantum magnets: Clinoatacamite, paratacamite, and herbertsmithite," *Applied Physics Letters*, vol. 98, no. 9, 2011, doi: https://doi.org/10.1063/1.3562010